CONF-780497--2

Presented at the Workshop on X-ray Instrumentation for Synchrotron Radiation Research, SLAC, Stanford, CA, April 3, 1978

LBL-7542

MASTER

SEMICONDUCTOR DETECTORS FOR FLUORESCENT EXAFS

F. S. Goulding, J. M. Jaklevic, and
A. C. Thompson

April 1978

Prepared for the U. S. Department of Energy
under Contract W-7405-ENG-48

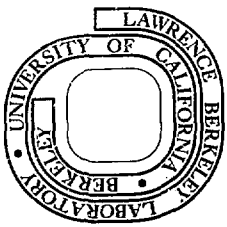

SEMICONDUCTOR DETECTORS FOR FLUORESCENT EXAFS*

F. S. Goulding, J. M. Jaklevic, and A. C. Thompson
Lawrence Berkeley Laboratory
University of California
Berkeley, California 94720

Introduction

Many papers have dealt with the mechanics of semiconductor detectors and of the associated electronics. We do not have the time or inclination to repeat much of this general material and will assume that our audience is at least familiar with the basic principles of the subject. Instead, we propose to address the subject of semiconductor detectors in the limited context of their use in Extended X-ray Absorption Fine Structure (EXAFS) studies using synchrotron radiation and to examine the special considerations which enter into their use in these applications.

We will further limit the topic to consideration of silicon detector systems. The only other material which might merit discussion is germanium, but the simple fact is that silicon detectors of readily available thickness absorb virtually all x-ray photons at energies produced by storage rings such as Stanford Positron Electron Accelerator Ring (SPEAR). Furthermore, the probability of escape of the detector material x-rays from the detector is much greater for germanium than silicon, so spurious peaks commonly occur in germanium detector x-ray spectra. Simply stated, cooled silicon detectors are almost ideal detectors for low energy x-rays and the alternative semiconductor materials offer nothing but disadvantages.

Fluorescence EXAFS

The silicon detector application which we have studied in some detail, and which forms the main subject of this paper, is to fluorescent EXAFS studies--that is EXAFS measurements where the detector observes the fluorescent x-rays emitted from the sample when exposed to incident exciting x-rays at energies just greater that the absorption edge of an element of an element of interest. Figure 1 shows the arrangement used in these experiments. Broadband synchrotron radiation from the storage ring is

*This work was supported by the Division of Biomedical and Environmental Research of the Department of Energy under Contract No. W-7405-ENG-48.

passed thorugh a monochromator which passes an almost monochromatic (i.e., ~1 eV spread) beam onto the sample. The actual energy selected by the monochromator can be varied by rotating the channel cut (or double) crystal in the monochromator. As the incident energy is varied past the absorption edge (usually K edge in our work), the EXAFS structure is observed both in absorption (the more common technique) and in the emission of x-rays characteristic of the element.

Figure 2 shows the EXAFS behavior observed both in absorption and in fluorescence when a biological specimen containing a low concentration of molydenum is measured. The EXAFS structure is quite clear above the Mo K-absorption edge in the fluorescence plot (i.e., counting only events in the Mo Kα radiation), while the absorption curve shows only a small step at the Mo edge. When properly analyzed, the absorption spectrum, with its excellent statistics, does reveal the same EXAFS structure but spurious peaks appear. Figure 3 illustrates the two spectra when suitably processed. Spurious peaks are clearly observed in the absorption case. This structure is most objectionable when trace elements are analyzed. For this reason, we have generally chosen to use the fluorescent EXAFS method in our work on trace elements in environmental and biological samples. The structure of the EXAFS curve is used to derive information on the chemical state of the element being observed.

In considering the requirements on the detector and signal processing system, some very particular aspects of the fluorescent EXAFS situation become important:

(i) EXAFS is a small perturbation on the gross elemental absorption curve and to discriminate small changes in the EXAFS requires very good counting statistics. Furthermore, EXAFS exist over a range ~1 keV in energy, and structure in the ~10 eV range of resolution may be important. Therefore, typical excitation scans consist of measuring 200 to 400 points, each of which must be measured with very good statistics. Expressed quantitatively, if the EXAFS amplitude is ~10% of the absorption edge step, a 1% determination of the EXAFS amplitude would require a total count of 10^6 in the characteristic fluorescent x-ray peak for each measurement point. If we allow 20 sec for each measurement (i.e., ~1 to 2 hours per scan), this implies a counting rate of 5×10^4 counts per second in the

fluorescent x-ray peak. Unfortunately, the detector also sees the Compton and Rayleigh scattered radiation mainly from the principal constituents of the sample (often carbon in our case). For trace quantities of the elements of interest, say 10 ppm, the counting rate in the elemental fluorescent peak may only be in the range of 0.1% of the total rate. Therefore, in the extreme case we are considering, the total detector counting rate must be ~5 x 10^7 c/s. For the reasons discussed later, this is not practical; fortunately, our demand for statistical accuracies of 1% of the EXAFS amplitude for each 5 eV point is excessive. If the structure does not contain components with such fine resolution several data points can be combined to improve statistics. With this in mind, and with some relaxation in the statistical accuracy requirement, excellent EXAFS data can be obtained with total counting rate of ~10^5 c/s. However, this discussion does focus attention on the great importance of being able to handle very high-counting rates while retaining good energy resolution--which is quite a different problem from that encountered in typical high-resolution semiconductor detector x-ray systems.

(ii) The need for high-counting rates implies that efficient detector geometries must be employed even with such intense x-ray sources as the SPEAR facility. Unfortunately, this means that the technique of reducing scatter radiation by observing only in the (horizontal) polarization plane cannot be employed. Therefore, large scatter peaks are observed in addition to the weak fluorescent x-rays. Figure 4 schematically shows a spectrum as observed by the silicon detector. The Rayleigh (coherent) and Compton (incoherent) scatter peaks consist of incident photons scattered mainly by the substrate of the sample containing the trace element which produces the fluorescent x-rays. Since the incident x-ray energy is varied during a complete EXAFS measurement, the separation of the Rayleigh (and Compton) peaks from the fluorescent x-ray peak changes during an experiment. In the worst case, when the incident x-ray energy just exceeds the absorption edge energy, the difference between the Rayleigh peak and the fluorescent x-ray energies is essentially the same as the difference between the 2p K-edge and the 3d L-edge energies of the element being analyzed (or L and M shells if an L-edge is being studied). The energy of the Compton-scattered photons depends on the scattering angle. Figure 5

shows the difference in energy between the Compton-scattered photons at 90° and 180° scattering angles and the K x-ray energy for various elements. The K x-ray energy is indicated horizontally in this figure.

This figure also shows the variation of energy resolution of typical silicon x-ray systems as a function of energy. Electronic energy resolutions of 150 eV and 250 eV are assumed in these curves--which of these numbers applies depends a great deal on the counting-rate demands placed on the system. Detector charge production statistics cause the increase in resolution as the energy increases. Since the number of counts in the Compton peak is always very large compared with that in the trace element fluorescent x-ray peak, the low-energy tail on the Compton peak can cause very serious interference with the fluorescent x-ray peak. Therefore, it is clear that the sensitivity of the method is critically dependent on the difference between the two sets of curves in Fig. 5 and that the best results are obtained for elements whose characteristic x-ray energies are in the 5 to 20 keV range.

A spectrum which illustrates the problems graphically is shown in Fig. 6. This particular spectrum was obtained when exciting a biological sample containing approximately 50 ppm of molybdenum with an incident x-ray energy of 20.2 keV. The spectrum illustrates the effect of using a niobioum filter to cut down the counting rate in the Rayleigh and Compton scatter peaks. Fortunately, the Mo Kα peak is well resolved from the Nb Kα peak caused by fluorescence in the niobium filter. The tail on the Compton scatter peak which falls lower in energy than the Nb K absorption edge, and which interferes with the Mo Kα peak, is most likely due to multiple Compton-scatter events in the sample or in the filter.

Detector and Pulse Processing System

This brief introduction to fluorescent EXAFS applied to trace element studies should serve as a guide to the important characteristics of silicon detector systems in this application.

The first obvious requirement is that the detector should be efficient at the energies of interest (say 1 keV to 25 keV). Figure 7 shows the variation of efficiency (photoelectric) for silicon detectors 3 and 5 mm thick. At the high-energy end of the range, the efficiency falls

off quickly and the 5 mm thick detector is clearly better if energies ≈25 keV are to be measured. As can be seen, at low energies the basic cut off is determined by an unavoidable silicon dead layer of about 0.2 μm at the entry window. The silicon K-edge absorption is clearly reflected this efficiency curve, but generally, the basic detector efficiency remains close to unity down to 1 keV (i.e., Na K x-rays). Figure 7 also shows the low energy cut-off due to the 1 mil Be window generally used as the cryostat entry window in an x-ray detector system (note that the detector must be operated at ~77°K to reduce its leakage current to an acceptable value). Also shown is the effect of 2 cm of air at atmospheric pressure. This emphasizes the need for using vacuum or helium paths in mos' low energy x-ray applications. As shown in these curves, silicon detectors provide efficient x-ray detectors in this energy range.

A second aspect of silicon detectors which deserves discussion is that of background produced by incomplete charge collection. At low energies (such as x-rays), trapping losses in the bulk silicon are negligible. However, electrical surface charges on the sides of the detector cause partial charge collection due to the internal field distortions they produce, as shown in Fig. 8. That portion of the charge reaching the surface becomes trapped and is released so slowly that it does not contribute to the signal measured in the usual spectrometer electronics. The result of this type of charge loss is illustrated in Fig. 9, where counts which should occur in the full energy peak are reduced in amplitude to form background in the energy range below the peak. This background can be important in all x-ray fluorescence applications, including fluorescent EXAFS, since very large numbers of counts are usually produced in the high energy scatter peaks and statistical fluctuations in the resulting low-energy background caused at lower energies interferes with measurement of the weak fluorescent lines. One method which largely eliminates this problem is to use the guard-ring detector shown in Fig. 10, where the effective detector volume is defined by internal electric field lines.

The conditions of fluorescent EXAFS requires excellent energy resolution at very high-counting rates. Figure 11 shows a typical high resolution x-ray system with the major elements identified for discussion of the behavior of resolution at high-counting rates. The pulsed-light

feedback (PLF) preamplifier allows signal charge (and leakage current) to accumulate on the feedback capacitor C_f until the preamplifier output reaches the threshold of the upper level discriminator (ULD) which then fires. This turns on the light emitting diode (LED) which causes drain-gate current in the field effect transistor (FET), thereby discharging C_f until the preamplifier output reaches the threshold of the Lower Level discriminator (LLD). The light is then turned off and the cycle starts again. Signals from the preamplifier are amplified, differentiated and integrated in the amplifier to produce Gaussian-shaped pulses at it output. More complex shaping systems can be used and may have slight advantages, but Gaussian shaping is suitable for this discussion. The amplifier output signals are inspected for pile-up and are only allowed through the linear gate when their amplitude is not affected by pile-up.

In such a system, the inspection time of the pile-up rejector must be greater than twice the signal (Gaussian) peaking time. As the input is increased, a bigger and bigger fraction of the events is rejected by the pile-up rejector. At very high input rates, all signals are rejected. Since the only useful signals are those passed on to the analysis system after pile-up rejection, it is important to operate at an input rate compatible with the shaping times used in the amplifier. Figure 12 shows the behavior of the input rate vs output rate for different pile-up inspection times. Note that the output rate peaks at an input rate equal to the reciprocal of the inspection time. Of particular interest in EXAFS work is the fact that the output rate may be independent or even a decreasing function of input rate depending on the point of operation of these curves. Therefore, to see EXAFS in the fluorescence mode, operation must be restricted to the reasonably linear part of these curves (i.e., input rate $<< 1/2T_I$ where T_I is the inspection time).

So far, we have not indicated the reasons for choice of a specific pulse width to be produced by the shaping circuits. Clearly, if the width were reduced, the system would be able to better handle high rates without pile-up problems. The choice of pulse width is constrained, in practice, by the effect of measurement time on resolution. Figure 13 illustrates the behavior of a typical system as a function of measurement time. Three sources of noise contribute to this behavior:

(i) Fluctuations in conduction in the FET channel cause "series" noise which increases at short measurement times. Generation and recombination processes in traps in the FET gate depletion layer also cause series noise.

(ii) Fluctuations in leakage current in the detector or FET cause "parallel" noise which increases at long measurement times.

(iii) Other noise sources cause a flat noise distribution which tends to be independent of measurement time.

The combination of these three terms results in an optimum measurement time which tends to be very long (~100 μs) in modern x-ray systems where the second term in very small. Such measurement times are not feasible for the high rates of EXAFS work and operation usually occurs where the first term (series noise) is dominant. Consequently, we will focus attention on the behavior of this term.

Series noise behaves as a noise voltage generator in series with the gate lead of the FET. Its value is given by the Nyquist relationship:

$$\overline{e_n^2} = 4KTR\,\Delta f$$

Where: Δf is the bandwidth integral of the system (i.e., $\int_0^\infty A(f)df$ where $A(f)$ is the frequency response)

and: R is the FET noise resistence ($\approx 1/g$ where g is the FET's mutual conduction).

We can therefore write:

$$\overline{e_n^2} = \frac{\phi^2}{gT}$$

where ϕ^2 is a constant

and T is a characteristic measurement time for the system.

$$\therefore \text{ rms noise } e_n = \frac{\phi}{\sqrt{gT}}$$

The equivalent detector charge is given by:

$$Q_{rms} = \frac{\phi C}{\sqrt{gT}}$$

The energy equivalent in the silicon detector is given by:

$$E_{rms} = \frac{\phi\epsilon}{q} \cdot \frac{C}{\sqrt{gT}}\ eV$$

and the FWHM energy resolution is therefore:

$$E_{FWHM} = \frac{2.35\ \phi\epsilon}{q} \cdot \frac{C}{\sqrt{gT}}\ \text{eV}$$

Assuming that ϕ is calculated for a Gaussian shaping network of peaking time T μs, and a temperature ~130°K is assumed, while g is expressed in mA/V and C in pF, this equation becomes:

$$E_{FWHM} \simeq \frac{121\ C}{\sqrt{gT}}\ \text{eV}$$

For example, if C = 5 pF, g = 5 mA/V and T = 1 μs, then $E_{FWHM} \simeq 270$ eV. These values are typical of the 2N4416 FET which is commonly used in x-ray spectrometers at low temperatures (~130°K). The final result shows the $1/\sqrt{T}$ dependence indicated in Fig. 13. It also shows the linear effects of capacity on resolution. This fact seriously restricts the detector area in high resolution systems to be used at high rates. Consequently, we have adopted the technique of using arrays of silicon detectors, each with its own preamplifier and electronics, for fluorescent EXAFS measurements. The system used in our early experiments is illustrated in Fig. 14A. A seven-detector system, proposed some time ago, is shown in Fig. 14B. The availability of 5 cm diameter silicon crystals of excellent detector quality has recently made the arrangement of Fig. 14C possible. All nine detectors in this proposed design are guarded for low background--either by neighboring detectors or by the outer guard ring. In addition to the improved background, this detector provides much better geometry than those of Figs. 14A and B.

This system would greatly increase the sensitivity for EXAFS measurements as compared with existing detectors. High-resolution work would be possible at total input rates greater than 250,000 counts/second. Using x-ray filters between the sample and detector, the analysis of very dilute specimens would greatly expand the application of the EXAFS to biological, environmental and physical chemistry.

A final remark should be made about potential improvements in semiconductor x-ray systems designed specifically for high-rate applications. While commericial FET's are limited to values of g/c in the range of 1 mA/V/pF, there is potential for development of germanium FET's exhibiting g/c values of as much as 10 mA/V/pF. As is indicated by the previous

calculations, such FET's should make possible substantial increases in counting rate while maintaining adequate energy resolution.

Acknowledgments

We thank D. Landis, N. Madden, J. Walton and D. Malone for assistance in developing the detector systems and electronics used in our experiments. Thanks are also due to M. Klein and his graduate students who have been associated with us in a number of experiments at the Stanford Synchrotron Radiation Laboratory.

Figures

1. Arrangement used in fluorescent EXAFS studies.
2. Basic data obtained by fluorescence and absorption measurements at the Mo K edge. The absorption data is expressed in terms of the effective absorption length derived from the ratio of intensities with (I) and without (I_0) the sample. Fluorescence data is expressed simply as the ratio of counts in the fluorescent peak (F) divided by the total flux (I_0) of incident photons.
3. EXAFS spectra extracted from the data of Fig. 2.
4. Schematic diagram showing the general features of the EXAFS spectrum.
5. Calculated energy differences between the Compton scattered radiation (at 90° and 180°) and the fluorescent K x-ray energies of various elements. It is assumed that the incident energy just exceeds the K edge at all points. Also shown are typical energy resolution curves for silicon detector spectrometers.
6. Typical EXAFS spectrum for a sample containing ~50 ppm of molybdenum.
7. Efficiency curves for silicon detectors.
8. Field distortions and poor charge collection in a normal silicon detector.
9. Illustrating the background at energies below the main scatter peaks in an x-ray fluorescence spectrum.
10. Illustrating a guard-ring detector.
11. Block diagram of typical x-ray spectrometer electronics.
12. Plot of input rate vs output rate in a system equipped with a pile-up rejector having various inspection times.
13. Resolution vs measurement time (i.e., peaking time for a Gaussian pulse shape) for a typical system. The left-hand scale is expressed in terms of N, the number of hole-electron pairs produced in a detector.
14. Detector configurations used and proposed for fluorescent EXAFS studies.

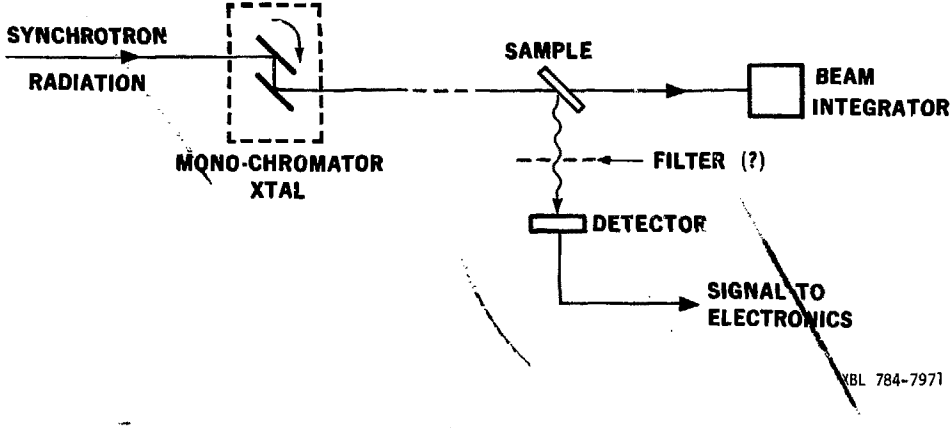
SYNCHROTRON
RADIATION
MONO-CHROMATOR
XTAL
SAMPLE
BEAM
INTEGRATOR
FILTER (?)
DETECTOR
SIGNAL TO
ELECTRONICS
XBL 784-7971

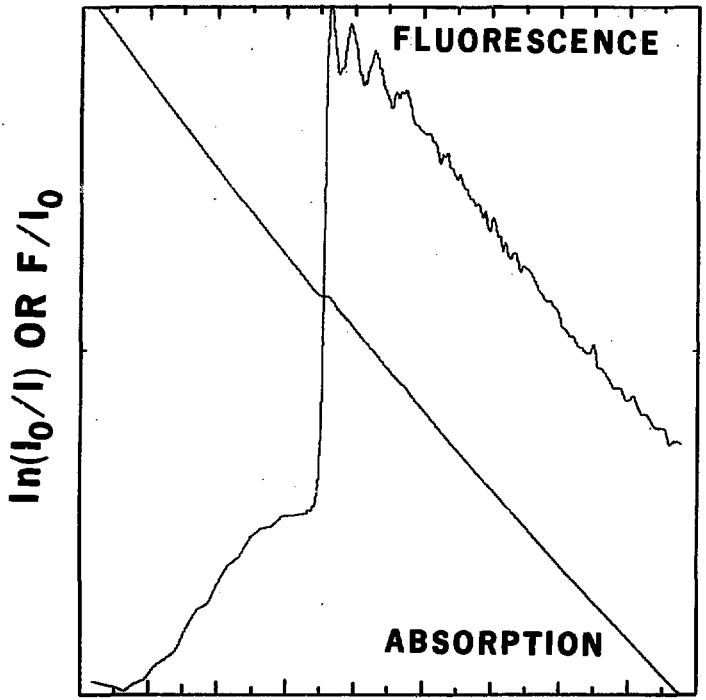

XBL 781-3783A

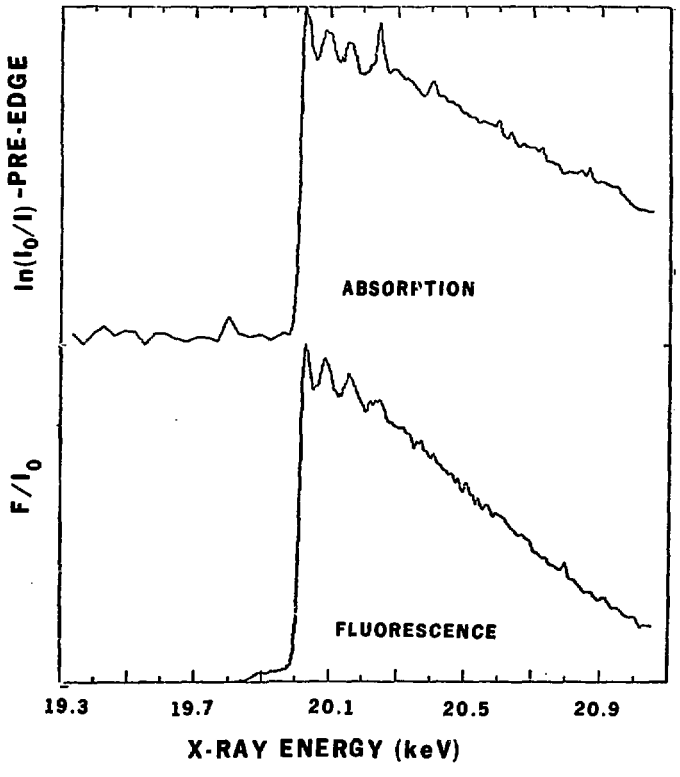
ln(I0/I) -PRE-EDGE
ABSORPTION
F/I0
FLUORESCENCE
19.3
19.7
20.1
20.5
20.9
X-RAY ENERGY (keV)

XBL 784-8189

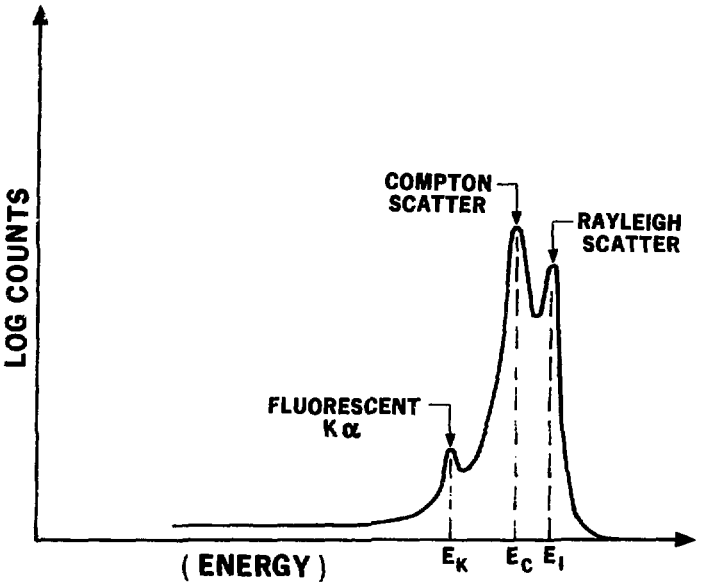
LOG COUNTS
COMPTON SCATTER
RAYLEIGH SCATTER
FLUORESCENT Kα
(ENERGY)
E_K
E_C
E_I

XBL 784-7968

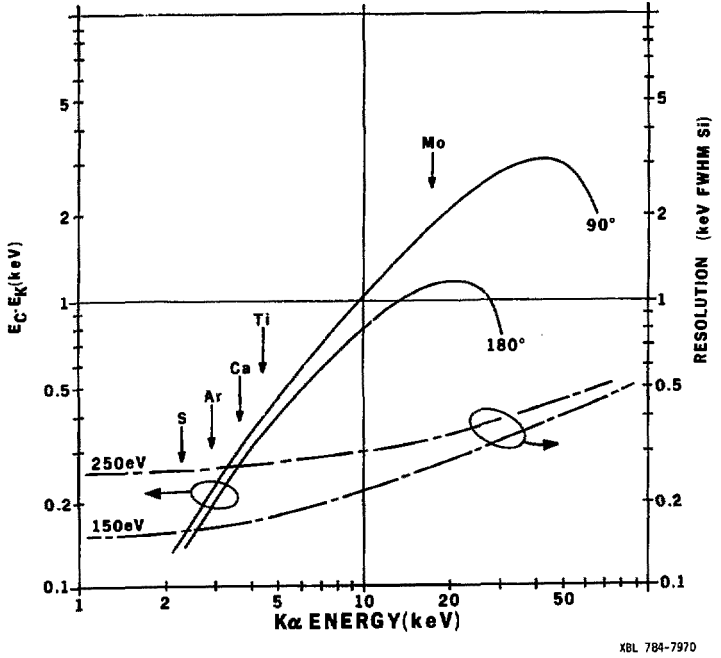
E_C-E_K(keV)
RESOLUTION (keV FWHM Si)
Kα ENERGY(keV)
Mo
90°
180°
Ti
Ca
Ar
S
250eV
150eV
5
2
1
0.5
0.2
0.1
1
2
5
10
20
50

XBL 784-7970

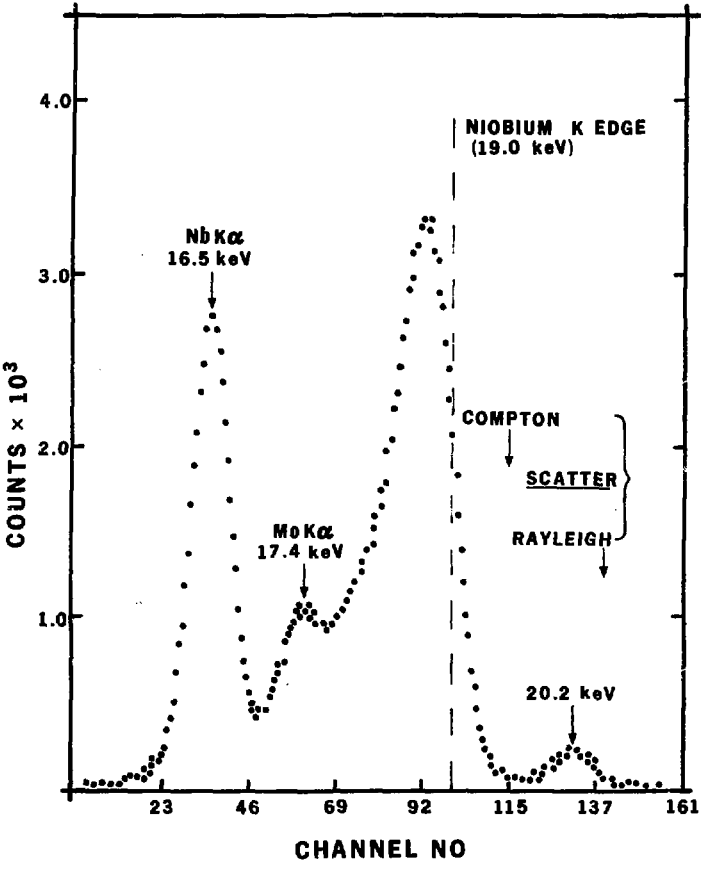
NIOBIUM K EDGE
(19.0 keV)
Nb Kα
16.5 keV
Mo Kα
17.4 keV
COMPTON
SCATTER
RAYLEIGH
20.2 keV
COUNTS × 10³
4.0
3.0
2.0
1.0
23
46
69
92
115
137
161
CHANNEL NO

XBL 784-7969

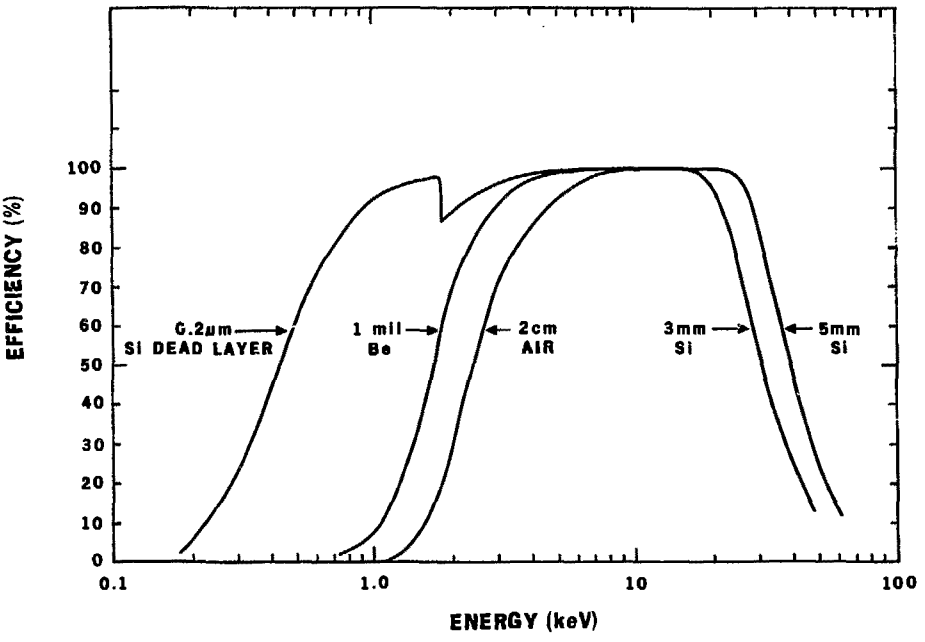
EFFICIENCY (%)
100
90
80
70
60
50
40
30
20
10
0
0.1
1.0
10
100
ENERGY (keV)
0.2μm
Si DEAD LAYER
1 mil
Be
2cm
AIR
3mm
Si
5mm
Si

XBL 784-7978

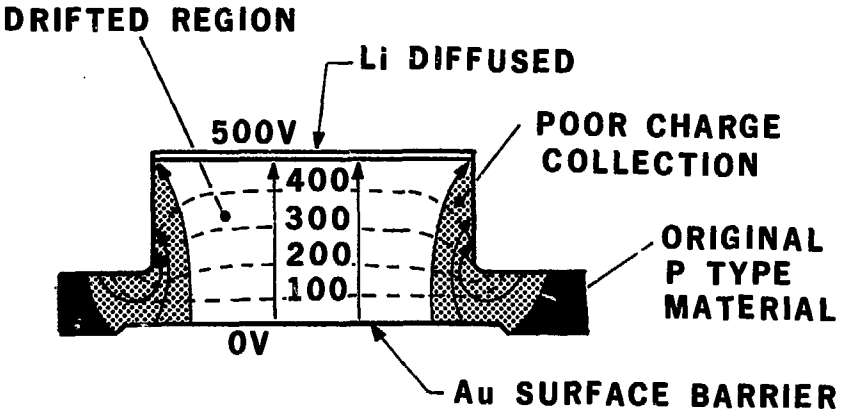
DRIFTED REGION
Li DIFFUSED
500V
POOR CHARGE COLLECTION
400
300
200
100
ORIGINAL P TYPE MATERIAL
0V
Au SURFACE BARRIER

XBL 784-7972

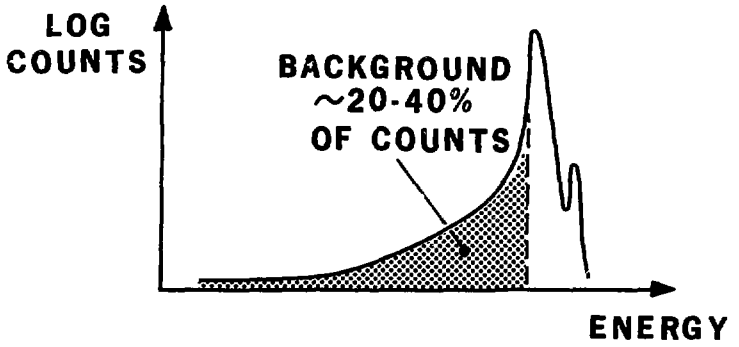

XBL 784-7974

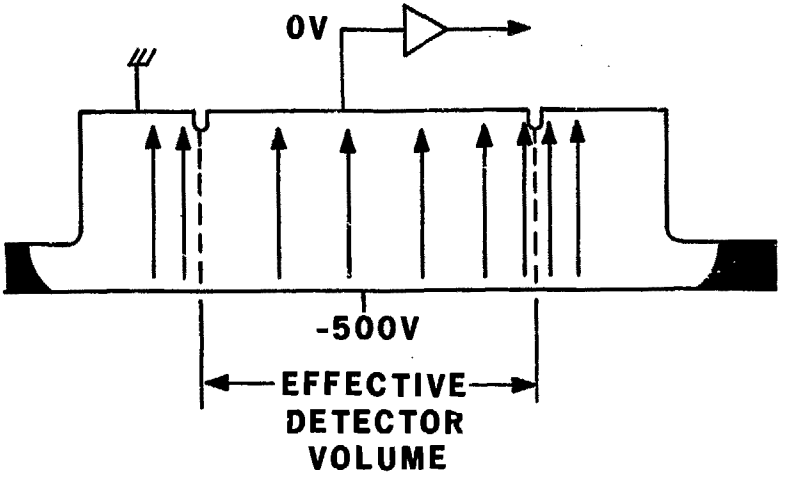

XBL 784-7973

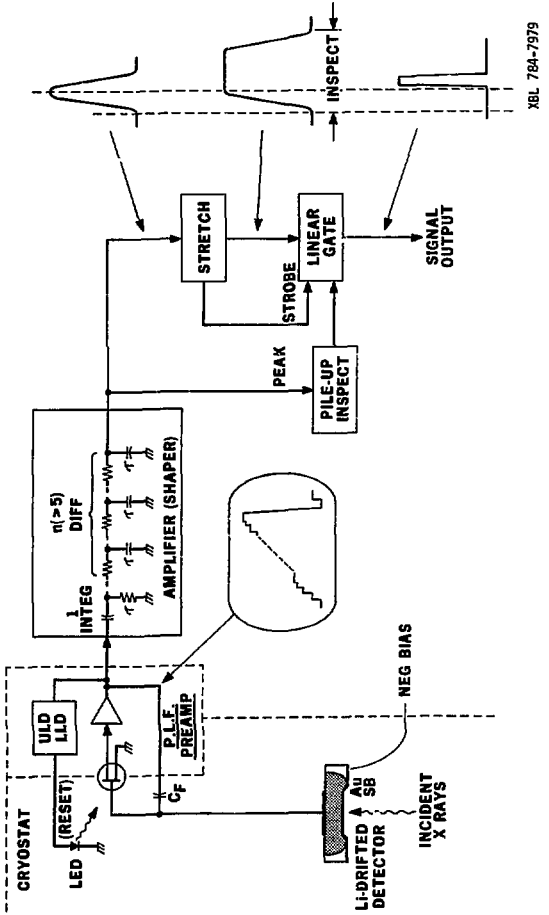
CRYOSTAT
LED
(RESET)
ULD
LLD
P.L.F.
PREAMP
C_F
NEG BIAS
Li-DRIFTED DETECTOR
Au SB
INCIDENT X RAYS
1 INTEG
n(>5) DIFF
AMPLIFIER (SHAPER)
PEAK
PILE-UP INSPECT
STROBE
STRETCH
LINEAR GATE
SIGNAL OUTPUT
INSPECT
XBL 784-7979

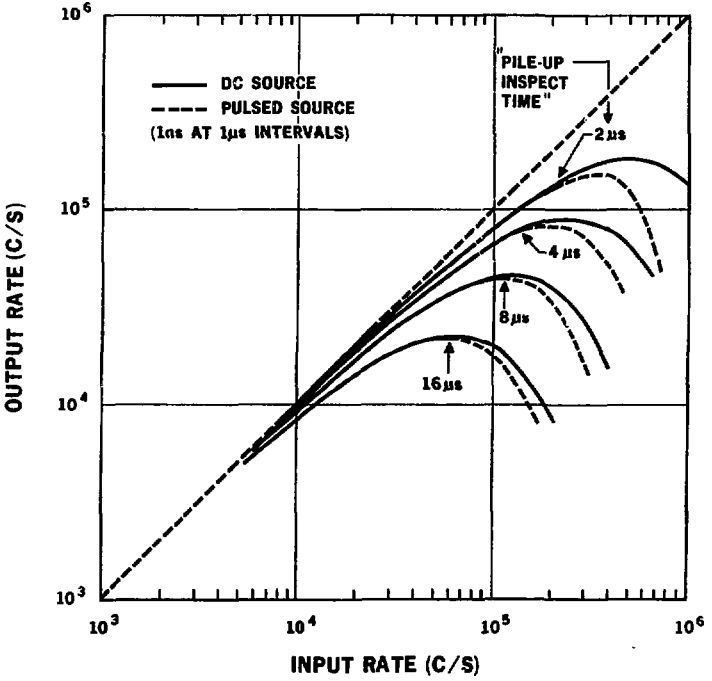
DC SOURCE
PULSED SOURCE
(1ns AT 1μs INTERVALS)
"PILE-UP INSPECT TIME"
2μs
4μs
8μs
16μs
OUTPUT RATE (C/S)
INPUT RATE (C/S)
10^3
10^4
10^5
10^6

XBL 784-7977

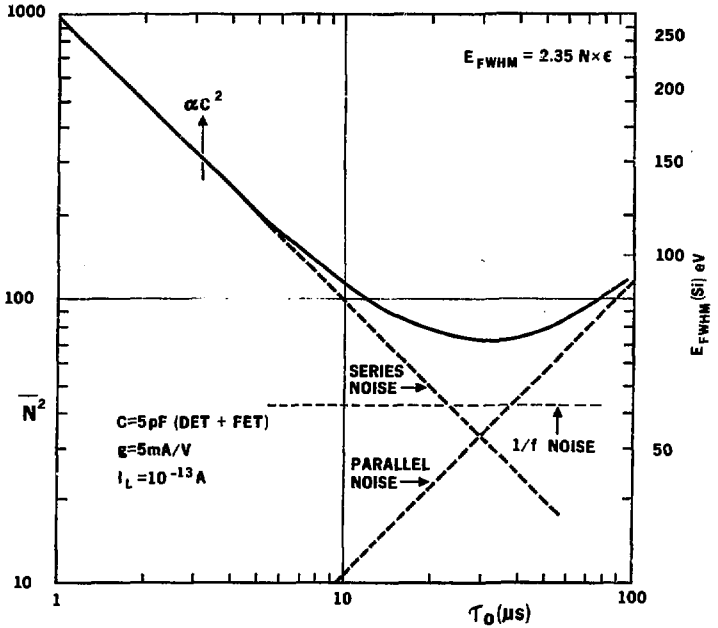
1000
100
10
$\overline{N^2}$
250
200
150
100
50
E_{FWHM}(Si) eV
$E_{FWHM} = 2.35\ N \times \epsilon$
$\propto C^2$
SERIES NOISE
1/f NOISE
PARALLEL NOISE
C=5pF (DET + FET)
g=5mA/V
$I_L = 10^{-13}$A
1
10
100
$\tau_0(\mu s)$

XBL 784-7975

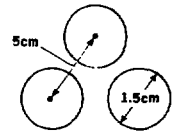

(A) 3 DETECTORS

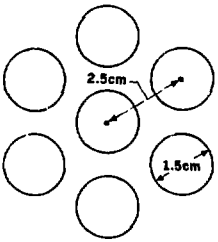

(B) 7 DETECTORS

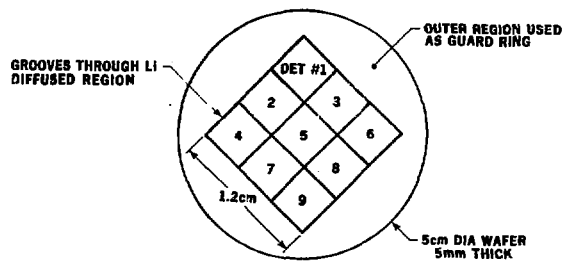

(C)

XBL 784-7976